SAND2020-2629C

CASL Thermal Hydraulic Hi2Lo Applications

Lindsay Noelle Gilkey

Structural & Thermal Analysis Group, Sandia National Laboratories, P.O. Box 5800, Mail Stop 0748, Albuquerque, NM 87185, lngilke@sandia.gov

INTRODUCTION

High-fidelity computational fluid dynamics (CFD) codes typically require significant resources and simulation runtimes, making detailed computational analysis expensive to perform. Low-fidelity thermal-hydraulics codes have a much lower computational cost, which makes them an attractive alternative to CFD in certain applications. High-to-low (Hi2Lo) is the concept of using higher-fidelity data from experiments and/or simulations to calibrate a lower-fidelity code to return results consistent with the higher-fidelity data.

The Hi2Lo process is discussed using the CFD code STAR-CCM+ (STAR) (high) and subchannel code CTF (low). Two applications were the focus of FY17, FY18, and FY19 milestones for CASL [1, 2, 3, 4, 5]. The first application used a Hi2Lo process to calibrate a mixing coefficient in CTF to match experimental and simulation data. The second application applied a mapping of the high-resolution data from STAR to CTF to replicate the higher-fidelity simulation data. This paper is a summary of the two applications.

MODEL GEOMETRY AND DESCRIPTION

The Hi2Lo applications were demonstrated with the Westinghouse Electric Company (WEC) 5×5 facility. The WEC 5×5 bundle experiments are a series of electrically heated rod bundle experiments. All rods are uniform in size and axial power shape. The radial power distribution is not uniform, as shown by Fig. 1, where the "dashed" rods have a higher relative power [6]. The experiment included either five mixing or non-mixing vane grids along the heated length of the geometry. Thermocouples were placed at the outlet to collect time-averaged temperature data of the 36 subchannels.

The boundary conditions for the corresponding STAR and CTF models were specified using outlet pressure, inlet temperature, mass flow rate, and the average linear heat rate per rod, defined as $AFLUX = Power/(LN_{rods})$, where L is rod length and N_{rods} is the total number of rods. Complete STAR and CTF model information is in [1, 2].

FIRST HI2LO APPLICATION: CALIBRATION OF CTF USING STAR

The first Hi2Lo application calibrated β, with $\beta = 0$ as the nominal case (no mixing between subchannels), to induce equivalent mixing in CTF and the experiment/STAR. β is a constant mixing parameter in CTF and adjusts turbulent mixing between bundle subchannels. It performs a similar function to a turbulence model in a CFD code. The non-mixing vane grid WEC 5×5 tests were used for this application. Half of the experimental data was reserved for validation; the other half was used for calibration. This is a summary of [1, 2].

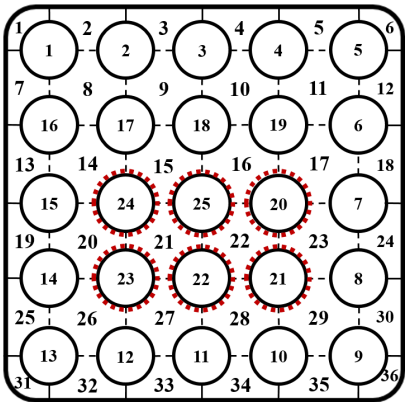

Fig. 1: WEC 5×5 exit cross-section with rod and subchannel numbering. The hot rods are dashed. Adapted from [6].

Bayesian Calibration and Experimental Design Method

The goal of the Hi2Lo calibration of CTF using STAR was to perform Bayesian calibration [7] of β. Dakota (Design Analysis Kit for Optimization and Terascale Applications) was used for all calibration steps, which is a toolkit for calibration and uncertainty quantification [8]. A surrogate was required to perform Bayesian calibration as the WEC 5×5 CTF model requires approximately 5 minutes to run a single core, which is expensive for Bayesian inference (typically $\sim 10^4$ evaluations) [9]. The steps used to build the surrogate are: 1) use Latin Hypercube Sampling (LHS) to generate CTF results at those input points, 2) reserve a subsampling of the LHS points, 3) build the surrogate model, excluding the reserved points, and 4) evaluate the surrogate using the reserved points to cross-validate the surrogate model.

Bayesian calibration was performed with the surrogate using the experimental data. 11,000 chains were collected and the first 1,000 samples were discarded to account for burn-in. Kernel density estimators (KDEs) were evaluated from the last 10,000 chains of the calibration. After the initial Bayesian calibration, an experimental design process was performed. The experimental design process steps are: 1) provide Dakota a list of existing design points, 2) use one experimental data point as an initial calibration point, 3) obtain the chain using the surrogate model, 4) the new chain is sent to Dakota, which selects a design point from the list provided in step 1, 5) this design point is added to the list in step 2, and 6) steps 3-5 repeat until Dakota uses all design points or meets a user-specified error tolerance. The experimental design process was performed using the STAR data (using an initial experimental data point for step 2) and then repeated using the experimental data as design point candidates.

Results and Discussion

The β values obtained from the initial Bayesian calibration and experimental design steps are shown in Tab. I. The experimental design KDEs are shown in Fig. 2a and 2b. Improvement was made statistically as the CTF L_2 norm decreased from the nominal case for all processes. However, it is hard to judge if improvement was made by performing the experimental design process over the initial Bayesian calibration. Both experimental design processes converged after 20 iterations and their most uncertain iteration was the initial point (Fig. 2a and 2b). However, the STAR data converged to $\beta = 0.002881$, and the WEC data converged to $\beta = 0.004025$. The STAR β is smaller than the WEC β, which is likely due to differences in response shapes between STAR and the experiment.

TABLE I: Summary calibrated β coefficients [1, 2].

Description	β	L_2 Norm
Nominal Case	0.0	1.44×10^{-2}
Bayesian Calibration	0.003197	1.36×10^{-2}
Experimental Design (STAR)	0.002881	1.36×10^{-2}
Experimental Design (WEC)	0.004025	1.36×10^{-2}

STAR and CTF show symmetry, as seen in Fig. 3. The CTF results are always symmetric due to a global β being used. The $\beta = 0$ nominal CTF case has no mixing between subchannels and has the flattest response. The STAR results are symmetric as there are no major geometric features in the non-mixing vane grid simulation that would induce asymmetry. The experimental data however is asymmetric. This may be caused by several factors, which includes potential thermocouple misalignment/damage or the presence of features in the actual geometry that would introduce asymmetry (e.g. dents or misaligned grids). There may also be a CFD modeling error, such as a coarse grid that is unable to resolve flow features. The STAR β is smaller than the initial Bayesian calibration and the WEC data β, which is likely due to the symmetry (and less crossflow) in the STAR simulation.

Milestones [1, 2] concluded that the Hi2Lo process was successful, however, a problem with greater sensitivity to the calibration parameters would have been more useful for demonstrating the Bayesian experimental design process. Improvements were made to the statistics compared to the nominal and the uncertainty in the β parameter was reduced as evidenced by the KDEs, however the relative insensitivity of the problem to β and the different trends in the CTF results and the experimental data made experimental design and calibration difficult with this specific application.

SECOND HI2LO APPLICATION: HI2LO MAPPING OF STAR RESULTS TO CTF

The second Hi2Lo application was to create an implementation of a surface map model between high-resolution surface temperature data from STAR to the lower-resolution subchannel code CTF. The surface map model generates high-resolution surface temperature data after being supplied simulation boundary conditions and low-resolution data obtained from CTF. The surface map model requires large volumes of data from STAR to train the model. This is a summary of the models described in [5].

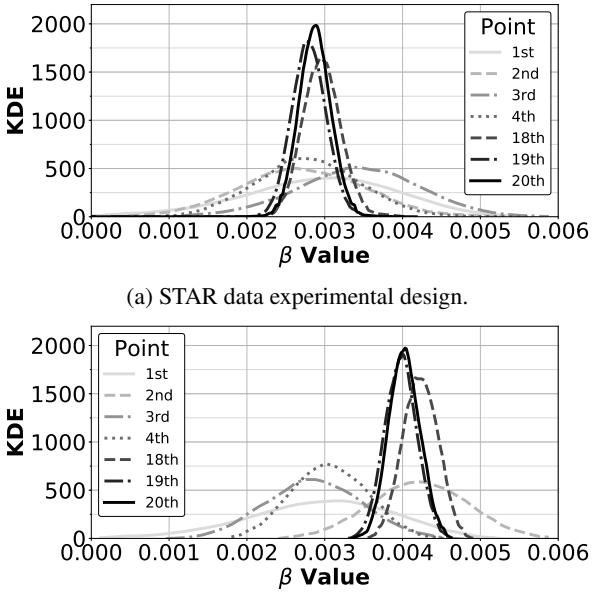

(a) STAR data experimental design.

(b) WEC data experimental design.

Fig. 2: Experimental design KDEs for β. Adapted from [9].

Summary of Models and Process

The surface map model is implemented in two steps. The first step is the TAVG map model which uses average temperatures from CTF ($TCTF_{avg}$) and the simulation boundary conditions to calculate an anticipated ratio of the STAR and CTF heat transfer coefficients at each CTF cell (multiplier M). The multiplier M is used to calculate the modeled average surface temperature from STAR (referred to as $TMODEL_{avg}$). The second step of the surface map model is the TSTAR map model which uses $TMODEL_{avg}$ and to predict the TMODEL values (which is at the same resolution as the STAR mesh). The TSTAR map model is beyond the scope of this summary paper and can be found in [5].

The TAVG map model imparts heat transfer, Q, calculated in STAR into CTF such that:

$$Q_{CTF} = Q_{STAR} \tag{1}$$

Since we assume that convection dominates the heat transfer from solid to the bulk fluid, Eqn. 1 was rewritten:

$$h_{STAR}A(\overline{T}_{w,STAR} - \overline{T}_{f,STAR}) = h_{CTF}A(\overline{T}_{w,CTF} - \overline{T}_{f,CTF}) \tag{2}$$

where h is the code convective heat transfer coefficient, A is the heat transfer area (assumed to be equal), $\overline{T}_w$ is the code average wall temperatures, and $\overline{T}_f$ is the code average bulk fluid temperature in the subchannel. If we assume the average bulk fluid temperature ($\overline{T}_f$) is equal in STAR and CTF, the heat transfer ratio (multiplier M) between codes is:

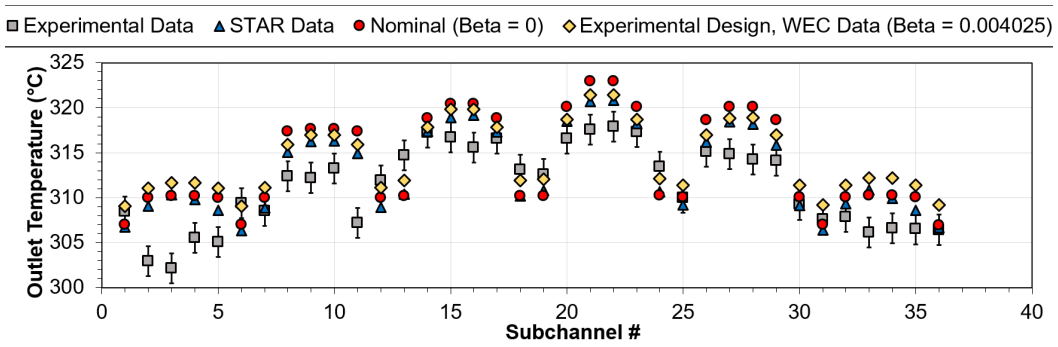

Fig. 3: Example comparison of the experimental, nominal, calibrated (WEC experimental design), and STAR outlet temperatures.

$$M = \frac{h_{STAR}}{h_{CTF}} = \frac{\overline{T}_{w,CTF} - \overline{T}_f}{\overline{T}_{w,STAR} - \overline{T}_f} \tag{3}$$

or in a form consistent with previous notation and using (θ, z) for spatial azimuthal and axial coordinates:

$$M(\theta,z) = \frac{\mathrm{TCTF_{avg}}(\theta,z) - \mathrm{TF_{avg}}(\theta,z)}{\mathrm{TSTAR_{avg}}(\theta,z) - \mathrm{TF_{avg}}(\theta,z)} \tag{4}$$

The TAVG map model should minimize the residual between $\mathrm{TSTAR_{avg}}$ and $\mathrm{TMODEL_{avg}}$. For the initial set of data, it is assumed that the same heat transfer ratio model for a given flow geometry and power distribution could be used if the same fluid properties were used in STAR and CTF and the flow is single phase. This assumption should be revisited as more data becomes available. The STAR data can be grouped by characteristic rod geometry (side, corner, or middle rod and vane orientation) and the mapping can be transformed on the θ coordinate to align the location of the subchannel walls (for the side and corner rods) and the mixing vanes to have the same orientation and placement relative to the subchannel walls. This methodology was chosen as it is useful when applying the surface map model from simpler to more complex geometry (e.g., applying from a 5×5 to a 17×17 rod bundle).

Results and Discussion

The model boundary conditions in Table II were run with the STAR and CTF 5×5 WEC models (with mixing vanes). Case 1 was the base case and was used for calibration of the surface map model. Cases 2 and 3 have different mass flow rates compared to Case 1. Cases 4 and 5 use a non-uniform axial power shape and Case 5 additionally uses a higher heat rate than the base case, which results in two-phase conditions. Table III summarizes the mean and max residuals found prior to (CTF residuals) and after (model residuals) applying the surface map model. All model mean and max residuals decreased significantly from the CTF residuals, including Case 5, which was two-phase. Milestone report [5] has significantly more discussion of results, including images and discussion of the higher resolution mapping.

[1] Non-uniform axial power shape used.

[2] Significant void/boiling observed in simulation results.

TABLE II: Boundary conditions used for the surface map model. Outlet pressure = 159.9 bar.

Case	Inlet Temperature (K)	Mass Flow Rate (kg/s)	Heat Rate (kW/m)
1	565.9	10.10	18.26
2	565.9	8.586	18.26
3	565.9	11.62	18.26
4	565.9	10.10	18.26[1]
5	584.0	10.10	22.82[1,2]

TABLE III: Results of $|\mathrm{TCTF_{avg}} - \mathrm{TSTAR_{avg}}|$ and $|\mathrm{TMODEL_{avg}} - \mathrm{TSTAR_{avg}}|$ for BCs in Tab. II.

Case	CTF Residuals (K)		Model Residuals (K)	
	|Mean|	|Max|	|Mean|	|Max|
1	9.0	12.6	0.68	2.7
2	10.3	14.3	0.79	3.2
3	8.1	11.2	0.60	2.4
4	10.9	16.7	1.7	5.5
5	9.6	16.9	5.6	11.3

Case 1 was used to train the surface map model and is expected to have small residual values for the surface map model. The "middle rods" (rod numbers 17 to 25 in Fig. 1) overall have the lowest model residuals (Fig. 4a). The surface map model is performed on rods grouped by geometry type rather than per individual rod, and these rods are generally more uniform in flow geometry than the side or corner rods.

Case 2 and 3 decreased or increased the mass flow rates through the bundle. Both cases use the same power distribution as Case 1 and have similar residuals. Case 4 and 5 have a non-uniform axial power distribution. Interestingly, Case 4 still has relatively low residuals, which implies that the heat transfer ratio between STAR and CTF (multiplier M) from Case 1 can be applied to Case 4 and return reasonable results.

Case 5 $\mathrm{TMODEL_{avg}}$ does not closely match the values for $\mathrm{TSTAR_{avg}}$, which can be seen in Tab. III and Fig. 4b. This is most likely because Case 5 has significant amounts of boiling, which drastically changed the heat transfer ratios when compared to Case 1, which was single-phase and used to train the surface map model. Additionally, the shape of the multiplier M is different between Case 1 and Case 5, as shown by

Fig. 5, which would make it unlikely that the same equation form could be used for the multiplier M. With additional two-phase STAR data, it may be possible to get better results for Case 5 and determine a better model for the multiplier M.

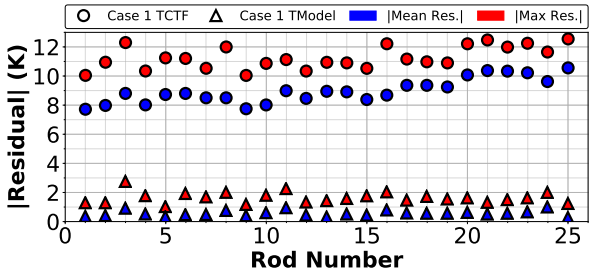

(a) Case 1.

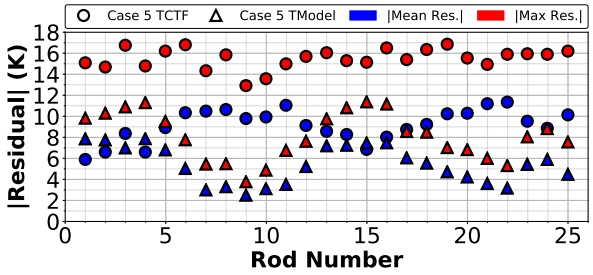

(b) Case 5.

Fig. 4: Comparing max and mean residuals of $|\text{TMODEL}_{\text{avg}} - \text{TSTAR}_{\text{avg}}|$ and $|\text{TCTF}_{\text{avg}} - \text{TSTAR}_{\text{avg}}|$.

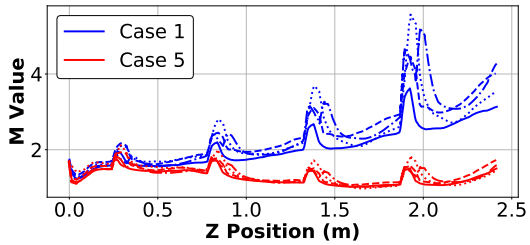

Fig. 5: Case 1 and Case 5 multiplier M values. Case 1 is single-phase. Case 5 is two-phase and has significant void/boiling.

The trained surface map model was able to reconstruct data that is similar to high-resolution data from STAR by performing the two-stage mapping process. For the 5×5 rod bundle data, the surface map model was able to adequately map the CTF data to a higher-resolution, however it did not perform as well for Case 5, which included two-phase data. Additional data is needed to evaluate if the surface map model can be trained to be able to include two-phase data. It may also be possible to include the surface map model in CTF directly on the single-phase flow and have CTF calculate the two-phase quantities, post single-phase mapping. Additional data and geometries should also be evaluated using the surface map model such as data from a 17×17 rod bundle. The inclusion of this data would allow us to see if the surface map model can be used to generate high-resolution data for a more complex geometry while leveraging a model trained on simpler geometry.

OVERALL CONCLUSIONS

Many milestones in CASL have focused on various Hi2Lo processes to varying degrees of success. Milestones [1, 3, 2, 4, 5] looked at two different methodologies of applying a Hi2Lo process from STAR to CTF to improve CTF predictions. Both approaches were relatively successful, however additional work can be performed to improve the results and more effectively demonstrate the processes. Both approaches/processes can be applied to different applications if opportunity or need arises.

ACKNOWLEDGMENTS

This work was performed with Natalie Gordon[1] and others. Thanks to Nathan Porter[1] and Aaron Krueger[1] for reviewing of this paper. Sandia National Laboratories is a multimission laboratory managed and operated by National Technology and Engineering Solutions of Sandia, LLC, a wholly owned subsidiary of Honeywell International, Inc., for the U.S. Department of Energy's National Nuclear Security Administration under contract DE-NA0003525. SAND2020-2629 C

REFERENCES

1. L. GILKEY, "STAR-CCM+ (CFD) Calculations and Validation," Sandia Technical Report SAND2017-12545 R, CASL (2017).
2. N. GORDON, "CTF (Subchannel) Calculations and Validation," Sandia Technical Report SAND2017-12874 R, CASL (2017).
3. L. GILKEY, "Surface Temperature Mapping Models for STAR and CTF," Milestone Report CASL-U-2018-1914-000, CASL (2018).
4. N. GORDON, "Average Surface Mapping Model Calibration," Milestone Report CASL-U-2018-1915-000, CASL (2018).
5. L. GILKEY, "Validation of Pin Span Superposition to Reconstruct Gridded Bundle Flows," Sandia Technical Report SAND2019-11787 R, CASL (2019).
6. P. F. JOFFRE, "Description of Mixing Vane Grid CHF test for CASL DNB Challenge Problem," Tech. Rep. PFT-16-3, Rev 1 (Propietary), Westinghouse Electric Company LLC (2016).
7. R. SMITH, *Uncertainly Quantification: Theory, Implementation, and Applications*, SIAM, Philadelphia, PA (2013).
8. B. ADAMS ET AL., "Dakota, A Multilevel Parallel Object–Oriented Framework for Design Optimization, Parameter Estimation, Uncertainty Quantification, and Sensitivity Analysis: Version 6.0 User's Manual," Sandia Technical Report SAND2014-4633, CASL (2014).
9. N. GORDON, L. GILKEY, R. SMITH, ET AL., "A Mutual Information–Based Experimental Design Framework to Use High-Fidelity Nuclear Reactor Codes to Calibrate Low-Fidelity Codes," *Nuclear Technology*, pp. 1–12 (04 2019).

[1] Sandia National Laboratories